Experimental characterization of 3D printed thermoplastic plates subjected to low velocity impact

Hari Prasad Prudhvi Desu, Anthony Rossi, Guneet Kaur Mankoo, Kazem Fayazbakhsh* and Zouheir Fawaz

Aerospace Engineering Department, Ryerson University, 350 Victoria Street, Toronto, ON, Canada M5B 2K3
**Corresponding author: kazem@ryerson.ca; Tel: (+1) 416-979-5000 ext. 6414; fax: (+1) 416-979-5056*

Abstract

3D printed parts made from PolyLactic Acid (PLA) have a brittle nature when subjected to out-of-plane loading, e.g. impact. In this paper, we report the use of a pendulum impact test apparatus along with a high-speed camera and an Infra-Red (IR) thermography system to investigate impact damage characteristics of PLA 3D printed plates. The effects of impact energy levels, impact locations, and changes in layer thickness were examined for a clamped plate with a raster angle of 0° and a nominal thickness of 2.52 mm. The upper impact energy level (3 J) showed higher absorbed energy percentage than the lower impact energy level (1 J) for two impact locations, namely central and off-center. For the 3 J impact energy, the maximum absorbed energy percentage for central loading was observed for specimens with 0.16 mm in layer thickness, while this occurred at 0.14 mm layer thickness for the off-center impact. For almost all layer thicknesses, the off-center loading resulted in a higher absorbed energy percentage compared to the central impact.

Keywords:

Fused Filament Fabrication (FFF); low velocity impact test; PolyLactic Acid (PLA); laminate fracture; energy absorption.

International Journal of Advanced Manufacturing Technology (2020) 107:1659-1669
https://doi.org/10.1007/s00170-020-05120-4

1. Introduction

Significant research work has been carried out on the structural performance of thermoplastic parts 3D printed using Fused Filament Fabrication technique (FFF). Among different manufacturing processes and design parameters, various studies specifically considered the effect of layer thickness, raster angle, and infill percentage on tensile strength and modulus of the final part. Researchers investigated tensile properties of 3D printed specimens per ASTM D638 and showed that lower layer thickness results in higher strength [1-5]. For example, Vidakis et al. [3] found an increase in tensile strength for ABS 3D printed specimens from 16.2 to 18.1 MPa when the layer thickness was decreased from 0.33 to 0.25 mm. Researchers examined the tensile strength and modulus of 3D printed test pieces using ASTM D638 and compared the test results with raster angles from 0° to 90° [6-8]. The results show that test pieces with raster angle of 0° have the highest tensile and modulus values. Several researchers investigated the effect of the air gap and infill percentage on tensile strength of 3D printed parts [9, 10]. Alvarez et al. [10] 3D printed specimens with an infill percentage linearly increased from 0 to 100% in increments of 5%, in which the maximum tensile strength and impact resistance was achieved at 100%.

While there are numerous studies on tensile strength and modulus of 3D printed parts, as can be seen from the quick summary presented above and the reviews by Popescu et al. [11] and Fayazbakhsh et al. [12], research studies investigating the effect of low velocity impact on 3D printed parts are rather limited. Caminero et al. [13] used a Markforged desktop 3D printer and manufactured samples out of nylon composites reinforced with continuous carbon, glass and Kevlar® fibers. They followed ASTM D6110 to evaluate their impact damage performance, and investigated the effect of layer thickness (0.1, 0.125, 0.2 mm), build orientation (on-edge and flat) and fiber volume content. For unreinforced samples, with an increase in layer thickness, they observed an increase in impact strength for flat samples, while there was a reduction for the case of on-edge samples. For reinforced composites, samples with on-edge build orientation showed higher impact strength compared to the flat ones. In a later study [14], they 3D printed Charpy impact specimens in flat, on-edge, and upright build orientations from three different PLA filaments, i.e. natural PLA, modified PLA (PLA 3D850), and PLA-Graphene. Samples with on-edge and flat build orientations showed higher impact strength compared to upright orientation. PLA and PLA 3D850 specimens showed 20 % to 30 % higher impact strength compared to PLA-Graphene samples in flat and on-edge orientations, while PLA-Graphene had similar or higher ductility in upright orientation compared to former specimens. Tsouknidas et al. [15] followed ISO 17340 standard (ductility testing for metallic materials) and investigated the effect of the following process parameters on the peak impact force: infill density, layer height, and filling pattern. Low density specimens displayed maximum impact energy per volume fraction at 0.1 mm layer height, and rectilinear filling improved kinetic energy dissipation at lower force rates. Roberson et al. [16] used a desktop 3D printer to manufacture samples out of ABS, PolyCarbonate (PC), PC-ABS, and ULTEM9085. They followed ASTM D256 to evaluate their impact resistance, and investigate the influence of build orientation and stress concentrator manufacturing (milling vs printing). They found the lowest impact resistance for printing along the Z direction and a lower variation in the test results for printed stress concentrator. Bax and Mussig [17] worked on biodegradable fiber reinforced PLA and showed that PLA/Cordeka composites have better tensile and Charpy impact

strength properties (DIN EN ISO 179) than PLA/Flax composites. Es-said et al. [18] worked on layer orientation of 3D printed ABS test pieces and showed high impact energy in 0° orientation (Average of 4.12 joules) compared to 45° and 90°. Caminero et al. [19] followed ASTM D7136 and performed an impact test on 3D printed composite specimens using a drop-weight tower. They manufactured a total of three specimens (150 mm × 100 mm) from glass fiber reinforced with nylon and used phase array ultrasonic testing to evaluate impact damage. For 20 J impact energy, specimens showed an average absorbed energy of 95% and a delamination damage at 1 mm depth from the impacted surface. While interesting, they did not investigate the effect of impact energy and only explored one set of 3D printing process parameters.

3D printed parts made from PLA have a brittle nature when subjected to out-of-plane loading, e.g. impact. At low impact energy levels, damage can arise in the subsurface through the thickness of the part and not be easily detectable. The previous research studies apart from [19] were limited in terms of test piece geometry and did not investigate low velocity impact of 3D printed plates and damage through the thickness. FFF technique introduces anisotropic properties to final parts and their mechanical behavior is governed by the same constitutive model used for fiber reinforced composite laminates. In low velocity impact of composite plates, damage mechanisms vary comprising both of intralaminar and interlaminar damage with their onset primarily initiated by the impact energy level. As a result, it is recommended that varying energy impact levels are utilized for experimental studies to identify the impact energy level damage thresholds [20]. While Caminero et al. [19] only considered central impact of 3D printed composite laminates, the impact location relation to the boundary edge conditions influences the damage severity. The impact location affects the degree of elastic (i.e. bending) and fracture energy (material failure) combinations, and subsequently the global response of the laminate. For composite plates manufactured using traditional techniques, Nassir et al. [21] found that off-center experiments had lower critical force and were more serious than central impact loading.

The experimental investigation undertaken in this paper incorporated test cases related to impact energy, impact location, and a 3D printing process parameter (i.e. layer thickness). In this paper, a pendulum impact testing apparatus along with passive Infra-Red (IR) thermography and a high-speed camera were used to investigate the impact damage characteristics of PLA 3D printed plates. Experiments on 3D printed PLA plates with varying impact energies (test plan #1) and layer thicknesses (test plan #2) were performed. In both sets, two impact locations were considered to investigate the influence of near boundary edge conditions. In the following sections, the test apparatus, specimen geometry and the test plans are first presented. Then, design and manufacturing parameters, among others, for fabrication of the specimens using FFF 3D printing are explained, followed by presentation and discussion of the results with finally some concluding remarks. The results obtained are useful for validating Finite Element simulation models of 3D printed parts in impact testing using impact energies and damage patterns obtained during testing.

2. Materials and Methods

In this section, the details of the test apparatus, test plans, testing procedure, boundary conditions and specimen manufacturing are presented.

2.1. Test apparatus

The pendulum impact test apparatus used in this study was designed in a previous research undertaking [22, 23] and acts like a drop-weight impact device per ASTM D7136. The impactor has a 16 mm diameter hemispherical striker tip, which weighs 4.4kg and is used to hit the required impact point of the test specimen. The test apparatus has two plates, namely a support plate and a clamping plate for mounting the test specimen. The test aperture is square in shape with a geometry of 114.5 × 114.5 mm (4.5 × 4.5 in).

The experimental setup is shown in Figure 1, depicting the impact test apparatus, the high-speed camera and the infrared camera. High intensity lights were also used to help enhance the recordings of the high-speed camera at 1000 Hz frequency. The impact velocity of the striker tip was calculated using the recording of the high-speed camera. The infrared camera was utilized to obtain the thermal response of the impact event from the back side of the test specimen. It had a resolution of 320 × 240 pixels, a temperature sensitivity of 20 mK, and a maximum recording frequency of 173 Hz.

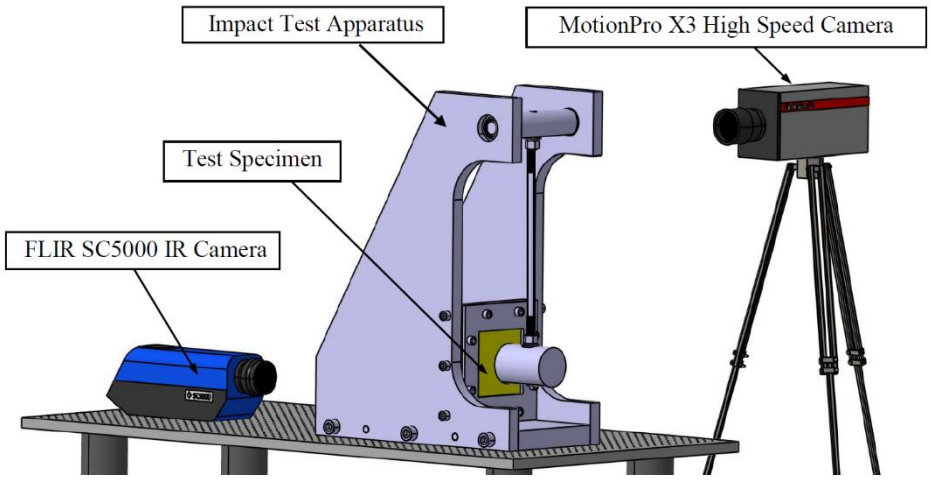

Figure 1. Experimental test set-up [22].

2.2. Specimen geometry, test plans, and energy calculation

The test specimens were 114.5 × 114.5 mm (4.5 × 4.5 in) square 3D printed PLA plates with raster angle of 0° and an overall thickness of 2.52 mm (0.10 in). The specimens were constrained on all four edges, and were subjected to impact at two different locations on the specimen. P_1 impact location is at the midpoint of the plate and P_2 location is at half the distance between the midpoint and the edge of the plate (Figure 2).

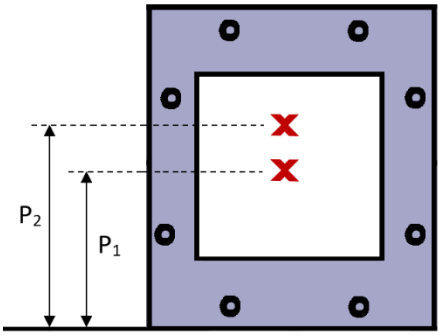

Figure 2. Two impact locations in the test plan (P_1 and P_2).

2.2.1 Impact energy threshold

To obtain the upper energy level for testing, impact energy levels of 5 and 4 J were first imparted at the center of the plates (point P_1), leading to a total breakage of the test plates into separate pieces in a circular pattern (Figure 3a). The test was repeated for 4 J energy level (Figure 3b) and a similar catastrophic failure/puncture was observed. As a result, the energy level was then reduced to 3 J at which point the plates only showed localized cracking without complete destruction. Plates were subsequently tested at this upper energy level as well as at a lower level of 1 J.

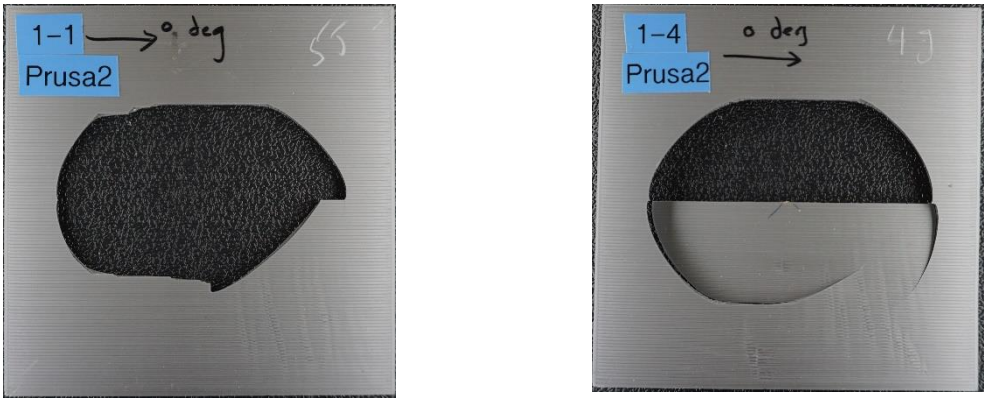

(a) **(b)**

Figure 3. Specimens after testing: (a) 4 J energy level and (b) 5 J energy level.

2.2.2 Test plan #1

The objective of the first test plan was to investigate the effect of varying impact location and impact energy, while the layer thickness of 3D printed specimens was fixed at 0.14 mm (a total of 18 layers and overall thickness of 2.52 mm). Two different impact energy levels of 1 J and 3 J at two different locations on the specimens (P_1 and P_2) were explored. Tests at a given impact energy level were repeated 3 times, resulting in a total of 12 tests. Table 1 specifies each test case according to the imparted impact energy and impact location on the specimen.

Table 1. Test plan #1 for low velocity impact of 3D printed PLA plates.

Test Case ID	Energy level (J)	Impact location
1a	1	P_1
1b	1	P_2
2a	3	P_1
2b	3	P_2

2.2.3 Test plan #2

For the second test plan, the layer thickness of 3D printed specimens was varied, while their overall thickness was kept almost constant at 2.52 mm (0.1 in). Four different layer thicknesses were used for 3D printing, i.e. 0.10 mm, 0.12 mm, 0.16 mm, and 0.18 mm. They correspond to an incremental decrease and increase in layer thickness compared to the test plan #1 (0.14 mm). The impact energy was fixed at 3 J and each configuration was tested with 3 samples and two impact locations resulting in a total of 24 samples. Table 2 summarizes the sample set configurations for this test plan.

Table 2. Test plan #2 for low velocity impact of 3D printed PLA plates with 3 J energy.

Test Case ID	Layer thickness, mm (number of layers)	Overall thickness (mm)	Impact location
1a	0.10 (25)	2.50	P_1
1b	0.12 (21)	2.52	P_1
1c	0.16 (16)	2.56	P_1
1d	0.18 (14)	2.52	P_1
2a	0.10 (25)	2.50	P_2
2b	0.12 (21)	2.52	P_2
2c	0.16 (16)	2.56	P_2
2d	0.18 (14)	2.52	P_2

2.2.4 Energy calculation

In the pendulum type of apparatus, when the pendulum is released, the potential energy is converted to kinetic energy, which allows the determination of the impact velocity (Figure 4).

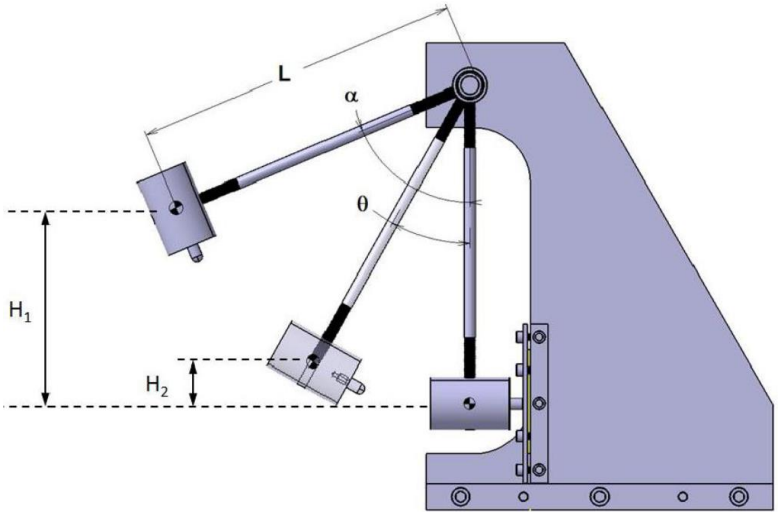

Figure 4. Pendulum impact test apparatus height set-up [23].

From Figure 3, the absorbed energy can be simply calculated using the initial potential energy of the striker (mgH_1) and its rebound energy (mgH_2):

$$\text{Energy absorbed} = m \times g \times (H_1 - H_2), \quad (1)$$

where m is the total mass of the pendulum and arm assembly, g is gravitational acceleration (9.81 m/s^2). H_1 and H_2 can be calculated knowing the pendulum arm length (L), and initial pendulum release (α) and rebound (θ) angles:

$H_1 = L \times (1 - \cos \alpha)$

$H_2 = L \times (1 - \cos \theta)$

The high-speed camera gives a live recording of the impact testing. Screen protractor software from Iconico was used to set the release angle (α) and measure the rebound angle (θ). The software provides two indicators: one is at a zero - degree angle (pendulum rest position), and the other was used to measure the release and rebound angles (Figure 5).

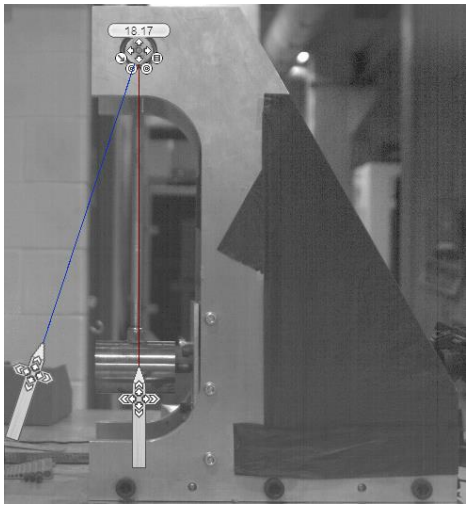

Figure 5. Screen protractor on the live recording.

2.3. Specimen manufacturing

19 specimens in total (including 7 spare ones) for test plan #1 and 24 specimens for test plan #2 were fabricated using a Prusa i3 MK2S 3D printer. Gray colored PLA filament from the same manufacturer (Prusa Research, Czech Republic) was used as the feedstock for 3D printing and Simplify3D software version 4.0 was used for G-code generation. The manufacturing process and design parameters are presented in Table 3 [12].

Table 3. Manufacturing and design parameters for 3D printing of PLA.

Manufacturing/design Parameter	Value	Manufacturing/design Parameter	Value
Build orientation[1]	XYZ	Bed temperature	60 °C
Raster angle	0°	Layer height	0.14 mm or see Table 1
Filament diameter	1.75 mm	Printing speed	2400 mm/min
Nozzle diameter	0.4 mm	Cooling	No fan cooling
Nozzle temperature	215 °C	Infill	100%

[1] Build orientation is defined per ISO/ASTM 52921:2013(E) [24].

Figure 6 shows a 3D printed PLA plate before testing. All manufactured specimens were tested using the apparatus described in Section 2.1 and the results are presented in Section 3.

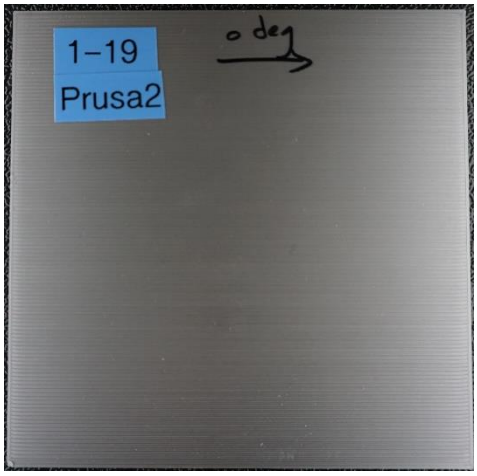

Figure 6. 3D printed PLA specimen before testing.

3. Results and discussion

This section summarizes the results of the impact testing for the two test plans: varying impact energy, and varying layer thickness. The damage pattern obtained from the IR camera, and absorbed energy and its percentage are presented.

3.1. Test plan #1

For the specimens tested at 1 J impact energy and two impact locations, the damage in the specimens was localized, and a crack or indentation could not be observed by the naked eye (Figure 7a and c). The damage can, however, be seen in the thermal images right after impact in the form of a crack along the direction of the extrudates, 0 deg (Figure 7b and d). This shows cracks in the interface between extrudates as opposed to cracking across them.

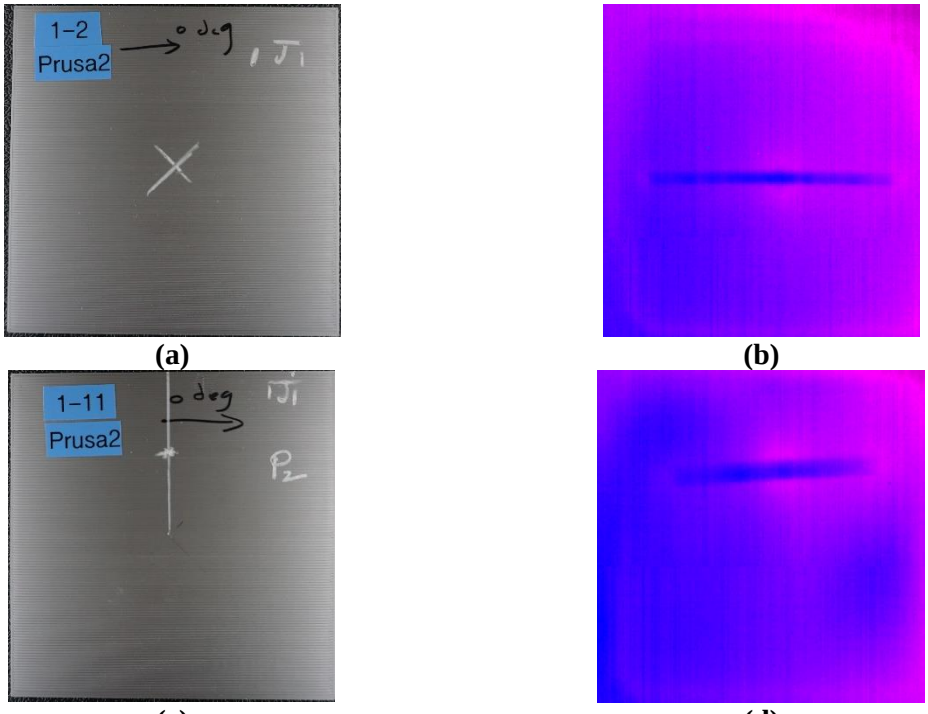

Figure 7. Specimens at 1 J energy level: (a) specimen after testing for P_1 impact location; (b) thermal imaging for P_1 impact location; (c) specimen after testing for P_2 impact location; and (d) thermal imaging for P_2 impact location.

For the 3 J impact energy and P_2 impact location, the specimens showed a variation in cracking which can be seen with the naked eye (Figure 8c). For P_1 impact location, in addition to a crack in the 0° direction along the extrudates (like the damage type observed for 1 J energy level), there is a crack along 90° and a semi-circular one (Figure 8b). Cracks are more extensive for P_2 impact location and multiple horizontal, vertical, and a circular damage pattern can be observed (Figure 8d). Therefore, it can be concluded that, at the upper impact energy level (3 J), in addition to cracks in the interface between extrudates, there is cracking across them.

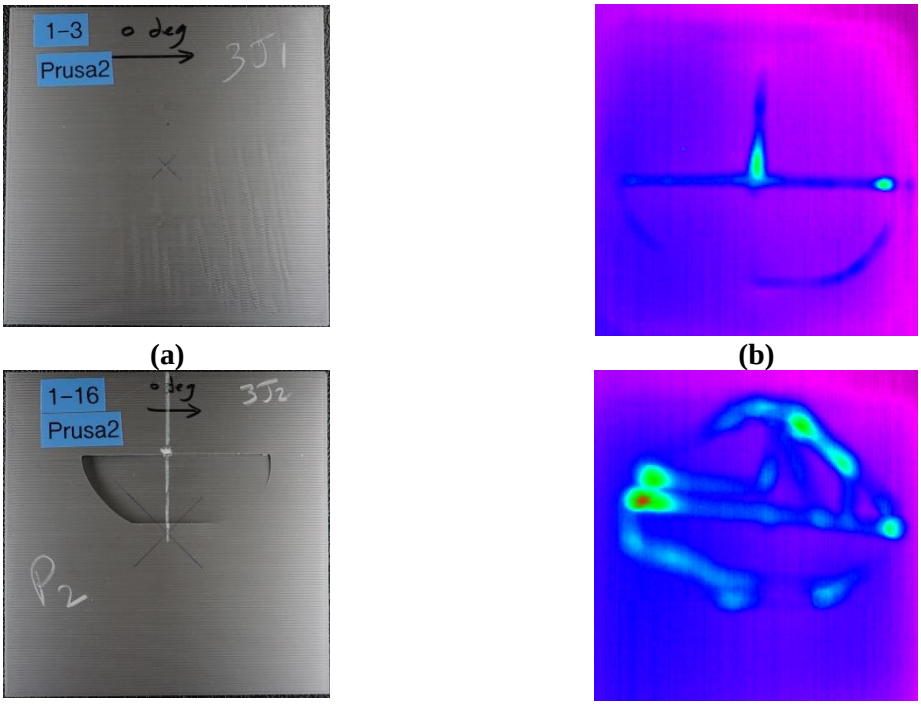

Figure 8. Specimens at 3 J energy level: (a) specimen after testing for P_1 impact location; (b) thermal imaging for P_1 impact location; (c) specimen after testing for P_2 impact location; (d) and thermal imaging for P_2 impact location.

In this low velocity impact testing, the impactor energy is transferred to the test specimens. If the entire energy is absorbed by the specimen, it will shatter the test part; however, depending on the conditions, the specimen may also transfer some of the momentum to the impactor causing a rebound. As a result, the impact energy is divided into the absorbed energy by the specimen and the rebound energy. The absorbed energy can be calculated using Eq. (2) below:

$$E\ (\text{absorbed}) = E\ (\text{total}) - E\ (\text{rebound}) \quad (2)$$

For one specimen, the calculations are explained in detail below to show how the release angle (α) and rebound angle (θ) can be used to get the absorbed energy value. For 1 J of impact energy with an impactor mass of 4.4 kg and acceleration due to gravity (g) as 9.807 m/s^2, the release height can be obtained from equation (3) as 0.0231 m:

$$E\ (\text{total}) = mgH_1 \quad (3)$$

Knowing H_1 and using equation (4), the release angle can be calculated:

$$\alpha = \text{Cos}^{-1}\ [1- (H_1/L)] \quad (4)$$

where L is 0.457 m for P_1 location and 0.428 m for P_2 location. As a result, the release angle can be calculated as 18.32°. For the first sample in the test case ID 1a (1 J impact energy and P_1 impact location), the rebound angle was measured at θ = 14° from high-speed videos analyzed by the screen protractor software. The rebound height H_2 can be calculated as:

$$H_2 = L\ (1- \text{Cos}\ \theta) \quad (5)$$

Knowing H_2, the rebound energy can be calculated using the same approach as equation (3). For the sample with θ of 14°, it is 0.585 J. Table 4 shows the impact energy, release angle, rebound angle, and rebound energy for each test specimen.

Table 4. Rebound angle and energy for test plan #1.

Test case ID	Impact energy (J)	Impact location	Impact angle α (°)	Rebound angle θ (°)			Rebound Energy (J)		
				Sample #1	Sample #2	Sample #3	Sample #1	Sample #2	Sample #3
1a	1	P_1	18.32	14.0	13.6	14.1	0.585	0.552	0.595
1b	1	P_2	18.94	15.6	15.7	15.2	0.680	0.689	0.646
2a	3	P_1	32.02	20.0	19.8	24.0	1.189	1.165	1.704
2b	3	P_2	33.12	5.0	6.0	5.8	0.070	0.101	0.094

Knowing the impact and rebound energies, the absorbed energy can be calculated using equation (2). The absorbed energy for the first sample in the test case ID 1a is: E (absorbed) = 1 - 0.585 = 0.415 J. The same procedure was followed for all the specimens and absorbed energy values and their percentages were calculated and presented in Table 5.

Table 5. Rebound and absorbed energies for test plan #1.

Test case ID	Rebound Energy (J)			Average rebound energy (J)	Absorbed Energy (J)			Average absorbed energy (J)	Absorbed energy percentage
	Sample #1	Sample #2	Sample #3		Sample #1	Sample #2	Sample #3		
1a	0.585	0.552	0.595	0.577	0.415	0.448	0.406	0.432	42.3
1b	0.680	0.689	0.646	0.672	0.320	0.311	0.353	0.328	32.8
2a	1.189	1.165	1.704	1.353	1.811	1.835	1.296	1.647	54.9
2b	0.070	0.101	0.094	0.088	2.930	2.899	2.912	2.912	97.1

The Maximum Normed Residual (MNR) method was used to screen the results in Table 5 for outliers. In this method, the maximum absolute deviation from the sample mean is divided by the sample standard deviation and the result is compared to the critical value for the sample size. The MNR for all test cases is below or equal to the critical value of 1.154 for the sample size of

three [25]. Therefore, all the test results were used for further analysis and investigation, e.g. average absorbed energy calculation.

Absorbed energy percentages for different impact energies and locations are plotted in Figure 9 showing average values and error bars.

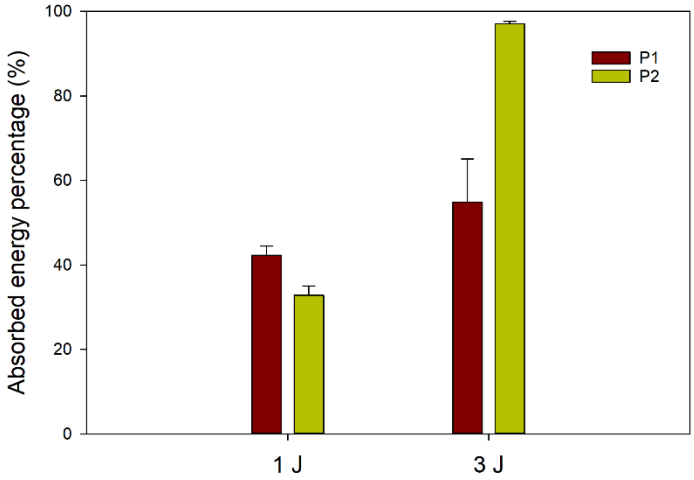

Figure 9. Absorbed energy percentage for test plan #1.

As seen in Table 4 and Figure 9, for 1 J impact energy, the absorbed energy for P_1 impact location is higher than the one for P_2 impact location, while this is the reverse for 3 J impact energy. At the upper impact energy level, absorbed energy percentage is higher for both impact locations compared to the lower impact energy level. Fracture in the specimens is a form of energy absorption; as a result, there is a correlation between crack length, and dissipated energy and its mechanism (Figure 7b and d). As can be observed, the crack length captured in thermal imaging is shorter for P_2 impact location (Figure 7d) compared to that for P_1 impact location, which correlates with absorbed energy percentages obtained in Table 4 (42.3% for P_1 impact location versus 32.8% for P_2). At 3 J impact energy, the damage type and pattern are more pronounced for P_2 impact location (Figure 8d), which translates into higher absorbed energy (97.1% for P_2 impact location versus 54.9% for P_1). The extensive cracks and damage patterns for P_2 impact location can be witnessed even by visual inspection.

Fracture along the extrudates (cracks in the interface between extrudates) dissipates less energy than that across the extrudates, where cracks change direction and orient themselves along 90 and 45-degree angles (Figure 8b and d versus Figure 7b and d, respectively). This indicates a change in the stress field from tensile loading to a mixed of tensile and shear as crack propagates and reaches plate clamped edges. Furthermore, the thermal images of the damage zone highlight significant temperature change when the cracks propagate along the 45° axis (Figure 8b and d) compared to the propagation along the 0° axis. Significant hot spots (high intensity and bright colors) appear where the cracks begin to change their orientations (from 0° to 90° and 45°), confirming more energy dissipation for a fracture under a mixed tensile and shear stress field. This

validates the results obtained in Table 4, where the absorbed energy percentage for 3 J impact energy and both impact locations is higher than the one for 1 J impact energy.

3.2. Test plan #2

In the test plan #1, experiments were performed with two different impact energies while specimens had the same layer thickness, 0.14 mm (18 layers total). The effect of impact energies and the crack behaviour were explored in detail. The upper impact energy level (3 J) induced more extensive damage and was selected for the second test plan. The same procedure discussed in the previous section was followed, and rebound and absorbed energies were calculated (Table 6).

Table 6. Rebound and absorbed energies for test plan #2.

Test case ID	Rebound Energy (J)			Average rebound energy (J)	Absorbed Energy (J)			Average absorbed energy (J)	Absorbed energy percentage
	Sample #1	Sample #2	Sample #3		Sample #1	Sample #2	Sample #3		
1a	1.462	1.268	1.050	1.260	1.538	1.732	1.950	1.740	58.0
1b	0.764	0.902	1.125	0.930	2.236	2.098	1.875	2.070	69.0
1c	0.587	1.451	0.595	0.591*	2.413	1.549	2.405	2.409*	80.3*
1d	0.776	0.893	0.693	0.787	2.224	2.107	2.307	2.213	73.8
2a	0.625	0.656	1.001	0.760	2.375	2.344	1.999	2.240	74.6
2b	0.510	0.425	0.430	0.455	2.490	2.575	2.570	2.545	84.8
2c	0.924	1.086	0.580	0.863	2.076	1.914	2.420	2.137	71.2
2d	0.523	0.915	1.006	0.814	2.477	2.085	1.994	2.186	72.8

*Sample #2 is an outlier and is removed from the calculations.

Like test plan #1, the MNR method was used to screen the results in Table 6 for outliers. The MNR for the test case 1c is 1.155, which is higher than the critical value of 1.154 for the sample size of three [25]. Therefore, sample #2 in the test case 1c is an outlier and is removed from the results. This is the only outlier in Table 6 and the rest of the results was used for further analysis and investigation, e.g. average absorbed energy calculation.

Absorbed energy percentages for P_1 impact location and different layer thicknesses are plotted in Figure 10 showing average values and error bars. With an increase in layer thickness,

there is an increase in absorbed energy percentage until 0.16 mm followed by a decrease in this value for 0.18 mm layer thickness.

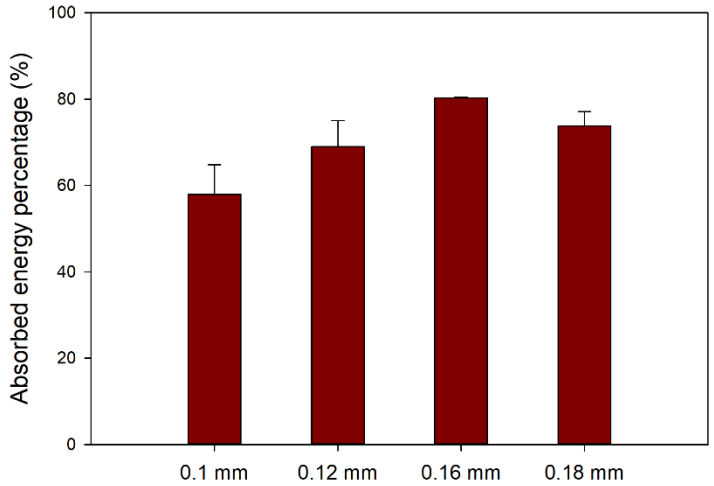

Figure 10. Absorbed energy percentage for test plan #2 and P_1 impact location.

Absorbed energy percentages for P_2 impact location and different layer thicknesses are plotted in Figure 11 showing average values and error bars. The same trend as Figure 10 can be observed here; however, the maximum absorbed impact energy occurs at 0.12 mm layer thickness.

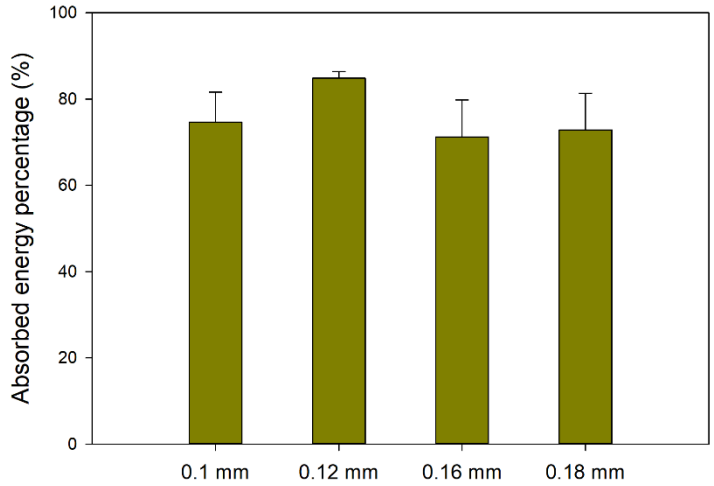

Figure 11. Absorbed energy percentage for test plan #2 and P_2 impact location.

The 3D printed plates are differentiated based on their stiffness, as defined by their geometric properties and boundary conditions. A detailed analysis of results suggests that the impact energy absorption of the plate is sensitive to the extrudate layer thickness of the plate and to a greater extent its influence on the global stiffness of the plate. The plate energy absorption mechanisms are affected by a complex structural response interaction between both material elastic energy and rupturing (fracture) energy. More specifically, for the plate impact structural response, there exists a transition state between elastic bending and rupture/cracking (induced between bending and transverse shear). If the bending stiffness of the plate exceeds a specific threshold value, the impact

energy dissipation is dominated by fracture energy with very little energy dissipation provided by elastic deflection. Also, worth mentioning that for a given layer thickness, the number of layers change so that the total laminate thickness remains constant (2.50 mm nominal). As a result, this is analogous to change in the fiber volume fraction and its effect on the interface fiber spacing. By restricting the matrix to small volumes flanked by the extrudents (fibers) gives rise to stress concentrations that initiate material fracture due to the localized stress exceeding material tensile limit. Also, the smaller matrix volumes give rise to interface fracture due to a reduction in the effective area to react the transverse shear, this damage is like what is classified as net shear-out type of failure. The brittle nature of the PLA material further exacerbates the damage initiation since there is hardly any stress relief due to lack of material plasticity. Hence, the complex loading interaction influenced by the geometric properties that may explain the behavior of the laminate structural response presented in Figures 10 and 11.

The same filament material and 3D printing process parameters were used in both test plans. As a result, specimens with 0.14 mm in layer thickness from test plan #1 can be combined with the results of test plan #2 (Table 7).

Table 7. Absorbed energy percentages for 3 J impact energy.

Layer thickness (mm)	Absorbed energy percentage at P_1	Absorbed energy percentage at P_2
0.10	58.0	74.6
0.12	69.0	84.8
0.14	54.9	97.1
0.16	80.3	71.2
0.18	73.8	72.8

Per Table 7, for P_1 impact location, there is almost an increase in absorbed energy percentage with an increase in layer thickness except for specimens with 0.14 mm in layer thickness. For P_2 impact location, with an increase in layer thickness, there is an increase in absorbed energy percentage until 0.14 mm followed by a decrease in this value. For almost all layer thicknesses, impact close to a clamp edge (P_2) results in a higher absorbed energy percentage compared to the impact to the plate center (P_1). This is expected since the off-center impact location (P_2) results in lower elastic deflection of the laminate plate, thereby yielding less rebound energy, or higher absorbed energy, than center impact (P_1). The maximum absorbed energy for P_1 impact location is 80 %, which occurs at 0.16 mm layer thickness, whereas this value is 97.1 % for P_2 impact location and 0.14 mm layer thickness.

It is worth noting that the experimental results of this study correlated well with existing published low velocity impact research work findings. Like Caminero et al. [19], the data suggests that the impact damage of the laminates is significantly influenced by the impact energy level and extrudate (fiber) thickness. Furthermore, as proposed by Cantwell and Morton [20], the phenomological effect of increasing the volume of the fibers does not necessarily increase its elastic absorption and was similarly captured by the experimental results of this study. With respect

to off-center impact locations, our experimental results for the upper impact energy level concluded similar findings to that of Nassir et al. [21] where the damage resistance of the plate diminishes compared to center impacts resulting in more severe damage (i.e., larger damage zone).

4. Conclusion

Impact testing of 3D printed PLA plates with different impact energies and locations, and layer thicknesses was performed. The testing was carried out using a pendulum impact apparatus, which was equipped with a high-speed camera and an infrared thermal imaging system. Two test plans were designed: two impact locations and two energy levels; and two impact locations and four different layer thicknesses. High-speed camera data were used to calculate the rebound and absorbed energies of the impact event, and thermal imaging was utilized to investigate damage mechanisms.

For the first test plan and lower impact energy level (1 J), cracks between extrudates were observed and the impact to the plate center dissipated more energy compared to the impact close to a clamped edge (42.3% versus 32.8%). For the upper impact energy level (3 J), cracks between and across extrudates were found, indicating a higher absorbed energy percentage compared to the 1 J impact energy tests, where only fracture dominated by tensile stress field was observed. Unlike the 1 J impact energy cases, the 3 J impact close to a clamped edge had higher absorbed energy compared to the impact to the plate center (97.1% versus 54.9%). For the second test plan, with an increase in layer thickness, there was an increase in absorbed energy percentage followed by a decrease in this value. For the impact to the plate center, the maximum absorbed energy percentage was 80 % for specimens with 0.16 mm in layer thickness, whereas this value was 97.1 % for the impact close to a clamped edge 0.14 mm layer thickness. Overall, at the upper impact energy level, the damage zone was larger for off-center impact locations compared to center impacts.

This work used test samples, where a plate with a raster angle of 0° was investigated. Specimens with other raster angles and stacking sequences, e.g. cross-ply, angle-ply, and quasi-isotropic could also be explored. In addition, different boundary conditions, e.g. a free edge is also worth exploring.

Acknowledgements

The financial support of this research work was provided by the Natural Sciences and Engineering Research Council of Canada (NSERC), RGPIN-2018-04144.

References

[1] Salem A, Singh M, Halbig MC (2015) 3-D printing and characterization of polymer composites withdifferent reinforcements. Advanced Processing and Manufacturing Technologies for Nanostructured and Multifunctional Materials II: Ceramic Engineering and Science Proceedings, Volume 36, (6): p. 115.

[2] Ning F, Cong W, Hu Y, Wang H (2016) Additive manufacturing of carbon fiber-reinforced plastic composites using fused deposition modeling: Effects of process parameters on tensile properties. Journal of Composite Materials. 51(4): p. 451-462.

[3] Vidakis N, Vairis A, Petousis M, Savvakis K (2016) Fused deposition modelling parts tensile strength characterisation. Academic Journal of Manufacturing Engineering. 14(2).

[4] Garg A, Bhattacharya A (2017) An insight to the failure of FDM parts under tensile loading: finite element analysis and experimental study. International Journal of Mechanical Sciences. 120: p. 225-236.

[5] Sood AK, Ohdar RK, Mahapatra SS (2010) Parametric appraisal of mechanical property of fused deposition modelling processed parts. Materials & Design. 31(1): p. 287-295.

[6] Riddick JC, Haile MA, Wahlde RV, Cole DP, Bamiduro O, Johnson TE (2016) Fractographic analysis of tensile failure of acrylonitrile-butadiene-styrene fabricated by fused deposition modeling. Additive Manufacturing. 11: p. 49-59.

[7] Carneiro OS, Silva AF, Gomes R (2015) Fused deposition modeling with polypropylene. Materials & Design. 83: p. 768-776.

[8] Ziemian S, Okwara M, Ziemian CW (2015), Tensile and fatigue behavior of layered acrylonitrile butadiene styrene. Rapid Prototyping Journal. 21(3): p. 270-278.

[9] Dawoud M, Taha I, Ebeid SJ (2016) Mechanical behaviour of ABS: An experimental study using FDM and injection moulding techniques. Journal of Manufacturing Processes. 21: p. 39-45.

[10] Álvarez K, Lagos RF, Aizpun M (2016) Investigating the influence of infill percentage on the mechanical properties of fused deposition modelled ABS parts. Ingeniería e Investigación. 36(3).

[11] Popescu D, Zapciu A, Amza C, Baciu F, Marinescu R (2018) FDM process parameters influence over the mechanical properties of polymer specimens: A review. Polymer Testing. 69: p. 157-166.

[12] Fayazbakhsh K, Movahedi M, Kalman J (2018) The Impact of Defects on Tensile Properties of 3D Printed Parts Manufactured by Fused Filament Fabrication. Mater. Today Commun. 18. 140–148.

[13] Caminero MA, Chacón JM, Garcia-Moreno I, Rodriguez GP (2018) Impact damage resistance of 3D printed continuous fibre reinforced thermoplastic composites using fused deposition modelling. Composites Part B: Engineering, 2018. 148: p. 93-103.

[14] Chacón JM, Caminero MA, García-Plaza E, Núñez PJ, Reverte JM, Becar JP (2019) Additive Manufacturing of PLA-Based Composites Using Fused Filament Fabrication: Effect of Graphene Nanoplatelet Reinforcement on Mechanical Properties, Dimensional Accuracy and Texture. Polymers. 11, 799.

[15] Tsouknidas A, Pantazopoulos M, Katsoulis I, Fasnakis D, Maropoulos S, Michailidis N (2016) Impact absorption capacity of 3D-printed components fabricated by fused deposition modelling. Materials & Design. 102: p. 41-44.

[16] Roberson DA, Perez ART, Shemelya CM, Rivera A, MacDonald E, Wicker RB (2015) Comparison of stress concentrator fabrication for 3D printed polymeric izod impact test specimens. Additive Manufacturing. 7: p. 1-11.

[17] Bax B, Müssig J (2008) Impact and tensile properties of PLA/Cordenka and PLA/flax composites. Composites science and technology. 68(7-8): p. 1601-1607.

[18] Es-Said OS, Foyos J, Noorani R, Mendelson Mel, Marloth R, Pregger BA (2000) Effect of layer orientation on mechanical properties of rapid prototyped samples. Materials and Manufacturing Processes. 15(1): p. 107-122.

[19] Caminero MA, García-Moreno I, Rodríguez GP, Chacón JM (2019) Internal damage evaluation of composite structures using phased array ultrasonic technique: Impact damage assessment in CFRP and 3D printed reinforced composites. Compos. B Eng, 165, 131–142.

[20] Cantwell WJ, Morton J (1991) The impact resistance of composite materials – a review, Composites, vol. 22(5), pp. 347-362.

[21] Nassir NA, Guan ZW, Birch RS, Cantwell WJ (2018) Damage initiation in composite materials under off-centre impact loading. Polymer Testing. 69: p. 456-461.

[22] Sy BL, Fawaz Z, Bougherara H (2017) Low Velocity Impact Assessment of Kevlar/Flax- Epoxy Composite Using IR Thermography, in CANCOM 2017.

[23] Sy BL, Fawaz Z, Bougherara H (2018) Damage evolution in unidirectional and cross-ply flax/epoxy laminates subjected to low velocity impact loading. Composites Part A: Applied Science and Manufacturing. 112: p. 452-467.

[24] ISO/ASTM 52921, Standard Terminology for Additive Manufacturing—Coordinate Systems and Test Methodologies. 2013. p. 1-13.

[25] MIL-HDBK-17F. Composite material handbook, Polymer matrix composite guidelines, vol. 1; 2002.